The effect of pressure on the crystal structure of NaV_6O_{11}

2008 J. Phys.: Condens. Matter 20 285208

(http://iopscience.iop.org/0953-8984/20/28/285208)

J. Phys.: Condens. Matter **20** (2008) 285208 (8pp) doi:10.1088/0953-8984/20/28/285208

The effect of pressure on the crystal structure of NaV_6O_{11}

Andrzej Grzechnik[1,3], **Yasushi Kanke**[2] **and Karen Friese**[1]

[1] Departamento de Física de la Materia Condensada, Universidad del País Vasco, E-48080 Bilbao, Spain
[2] Advanced Nano Materials Laboratory, National Institute for Materials Science, 1-1 Namiki, Tsukuba, Ibaraki 305-0044, Japan

E-mail: andrzej.grzechnik@ehu.es

Received 9 April 2008, in final form 22 May 2008
Published 17 June 2008
Online at stacks.iop.org/JPhysCM/20/285208

Abstract

The crystal structure of NaV_6O_{11} stays hexagonal at least to 8.06 GPa at room temperature as deduced from x-ray powder and single-crystal diffraction data measured in diamond anvil cells. The material is more compressible along the c axis and the distortion of the hexagonal close packing increases on compression. Its compressibility is given by a Murnaghan equation of state with the zero-pressure bulk modulus $B_0 = 177(9)$ GPa and the unit-cell volume at ambient pressure $V_0 = 369.9(4)$ Å^3 ($B' = 4.00$). The occurrence of the pressure-induced second-order $P6_3/mmc \rightarrow P6_3mc$ phase transition has been discussed on the basis of symmetry-mode analysis of the high-pressure single-crystal data.

1. Introduction

NaV_6O_{11} was first synthesized by electrolysis of a molten salt [1]. Since the discovery of its anomalous resistivity [2, 3], magnetic character [3], and structural phase transitions [4], the compound has received wide interest.

At ambient conditions, the crystal structure of NaV_6O_{11} ($P6_3/mmc$, $Z = 2$) [5] consists of hexagonal close-packed layers of O and Na atoms, and of three types of V atoms (figure 1). The $V(1)O_6$ octahedra form a regular Kagomé lattice perpendicular to [001] by edge sharing. The $V(2)O_6$ octahedra form a face-sharing dimer across a mirror plane perpendicular to [001]. The center of the trigonal bipyramid $V(3)O_5$ is in the mirror plane. The V(1) layer and the V(2)/V(3) layer alternate along [001]. The Na atoms are coordinated by 12 oxygen atoms in NaO_{12} dodecahedra. A Madelung energy calculation suggests that the V^{3+} cations prefer the V(1) site, while the V^{4+} cations reside at the V(2) and V(3) sites. The material is a Curie–Weiss paramagnetic metal at ambient conditions [3].

At $T_H = 243$ K, NaV_6O_{11} shows a second-order $P6_3/mmc \rightarrow P6_3mc$ structural phase transition, in which the mirror plane perpendicular to [001] is lost [4]. In the low-symmetry phase, the $V(1)O_6$ octahedra form trimers with a regular triangular shape. The ^{51}V-NMR study revealed that the V(1) atom shows a spin gap character with a spin-singlet ground state, while the V(2) and V(3) atoms maintain their local magnetic moments [6, 7].

At 80 K, NaV_6O_{11} undergoes a second structural phase transition to the orthorhombic phase $Cmc2_1$ ($Z = 4$) [4, 8, 9], in which the $V(1)O_6$ trimers distort into isosceles triangles. Although space group $Cmc2_1$ is a minimal subgroup of $P6_3mc$ and the experimental observations suggested a second-order character of the phase transition [4], Iwata and Ishibashi pointed out that the transition must be of the first order to fulfill the Landau condition [8].

Below $T_c = 64.2$ K, NaV_6O_{11} exhibits a uniaxial magnetic anisotropy with the easy axis of magnetization parallel to [001] [3]. According to electronic structure calculations [10, 11], the unpaired electrons reside at the V(2) and V(3) sites and couple ferromagnetically through the $V(1)O_6$ Kagomé layers, which act as a spin polarization medium.

The effect of pressure on the magnetization and the Hall coefficient in NaV_6O_{11} to 1.20 GPa was examined by Naka *et al* [12]. It turned out that the T_c temperature decreases, while the T_H temperature increases upon compression. Here in this study, we are interested in the structural stability of this mixed valence vanadate upon compression to about 8 GPa studied by x-ray powder and single-crystal diffraction in diamond anvil cells. We also aim to introduce a novel method to refine high-pressure diffraction data based on symmetry-mode analysis.

[3] Author to whom any correspondence should be addressed.

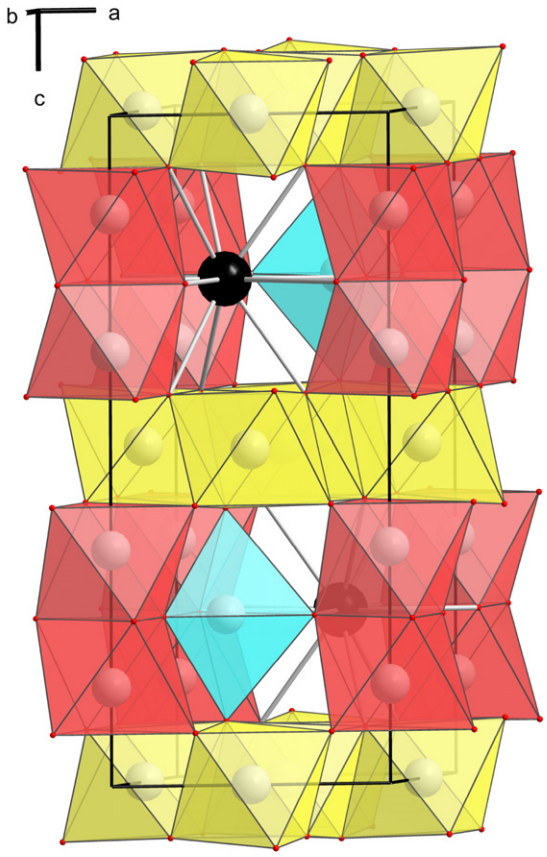

Figure 1. Crystal structure of NaV_6O_{11} ($P6_3/mmc$, $Z = 2$) at ambient conditions. The polyhedra around the V are drawn. Sodium atoms are represented by black symbols.

(This figure is in colour only in the electronic version)

2. Experimental details

The synthesis of opaque black single crystals of NaV_6O_{11} was described in [4] and [5]. A few of the crystals were finely ground in acetone for x-ray powder diffraction measurements.

High-pressure powder diffraction experiments at room temperature were performed using a Stoe IPDS II diffractometer at the 'single-crystal diffraction' beamline at the Institute for Synchrotron Radiation (ANKA, Karlsruhe Research Center, Germany). The sample was loaded into a DXR-6 Diacell diamond anvil cell for experiments with monochromatic radiation at 0.75 Å. The ruby luminescence method [13] was used for pressure calibration and isopropanol, which is chemically inert with respect to the vanadate, was used as a pressure medium. The two-dimensional powder diffraction diagrams were measured in the range $2\theta = 4°$–$33°$ and integrated with the Stoe software[4] to yield intensity versus 2θ diagrams. A fluorite powder was added as an internal standard for the 2θ calibration at each pressure through the CaF_2 equation of state [14].

Single-crystal intensities were measured using a Stoe diffractometer IPDS-2T with the Mo Kα radiation in an Ahsbahs-type diamond anvil cell (the opening angle of 90°) [15] at room temperature. The diamond culets (600 μm) were modified by laser machining so that the angle between them and the tapered parts of the diamonds was 40°. A 250 μm hole was drilled into a stainless steel gasket preindented to a thickness of about 100 μm. The intensities were indexed, integrated, and corrected for absorption using the STOE software (see footnote 4). Shaded areas of the images by the diamond anvil cell were masked prior to integration. The intensities were integrated simultaneously with three orientation matrices, corresponding to the crystal of NaV_6O_{11} and to the two diamonds of the cell. Due to their hemispherical shape, no absorption correction was necessary for the diamond anvils. The ruby luminescence method [13] was used for pressure calibration and isopropanol was used as a hydrostatic pressure medium to 4.20 GPa [16].

[4] STOE & Cie GmbH, Darmstadt.

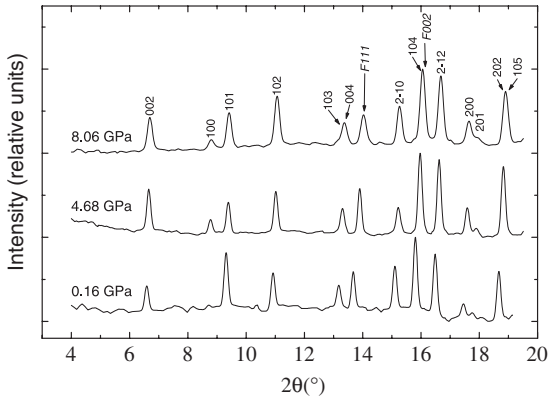

Figure 2. Selected x-ray powder diagrams in the range $2\theta = 4$–$20°$ at different pressures ($\lambda = 0.75$ Å). Symbols are the Miller indices of the observed reflections in space group $P6_3/mmc$. The (111) and (002) reflections due to CaF_2 are indicated as $F111$ and $F002$, respectively.

3. Results and discussion

Figure 2 presents three different x-ray powder diagrams up to 8.06 GPa at room temperature. The diagrams show no evidence for any phase transitions in this pressure range, i.e., there is no *hkl* dependent broadening of the reflections and no new reflections appear. Since our powder data do not allow us to distinguish space groups $P6_3/mmc$, $P6_3mc$, and $P\bar{6}2c$, we thus indexed all the observed reflections in space group $P6_3/mmc$ up to 8.06 GPa.

The lattice parameters and the unit-cell volume of NaV_6O_{11} ($P6_3/mmc$, $Z = 2$) at room temperature and ambient pressure are 5.7123(1) Å, 13.0974(4) Å, and 370.12(1) Å^3, respectively. The $(c/a) * (2/3)$ value of 1.529 is smaller than the ideal *hcp* value of 1.633, indicating that the structure is compressed along the [001] direction compared to the ideal hexagonal close packing. The pressure dependence of the normalized hexagonal lattice parameters, c/a axial ratios, and unit-cell volumes ($P6_3/mmc$, $Z = 2$), extracted from the powder diagrams using the Le Bail method implemented in the program JANA2000 [17], is presented in figure 3. NaV_6O_{11} is more compressible along the c axis and, hence, the distortion of the hexagonal close packing increases on compression. Its

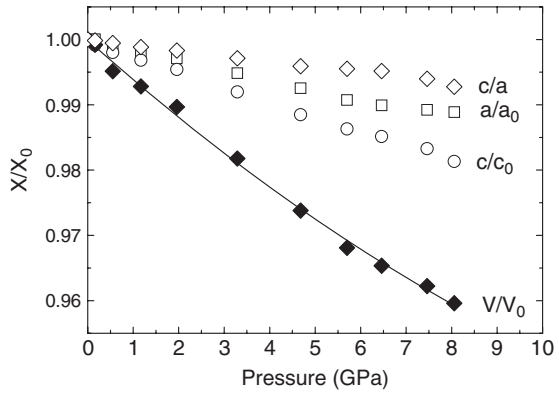

Figure 3. Pressure dependence of the normalized lattice parameters, c/a axial ratios, and unit-cell volumes. The solid line is a Murnaghan equation-of-state fit to the compressibility data.

compressibility data could be fitted by a Murnaghan equation of state with the zero-pressure bulk modulus $B_0 = 177(9)$ GPa and the unit-cell volume at ambient pressure $V_0 = 369.9(4)$ Å^3 (for the fixed first pressure derivative of the bulk modulus $B' = 4.00$).

At ambient pressure, the unit-cell volume of NaV_6O_{11} at 200 K ($P6_3mc$, $Z = 2$) is 368.66 Å^3 [4]. Based on our equation of state, the temperature-induced volume change at 200 K would correspond to compressing the material to 0.60 GPa at room temperature. Hence, the phase transition $P6_3/mmc \rightarrow P6_3mc$ would occur at pressures slightly lower than 0.60 GPa. However, according to the results presented in [12], the anomaly in the magnetic susceptibility associated with the *centrosymmetric* → *non-centrosymmetric* transition should take place at pressures higher than 1.15 GPa at room temperature.

The information content in both single-crystal and powder high-pressure diffraction data is in general limited due to a finite opening angle of every diamond anvil cell, always resulting in a low *reflection-to-parameter* ratio in structural refinements. In addition, second harmonic generation measurements to detect the absence of centrosymmetry in NaV_6O_{11} are not feasible because the crystals are non-transparent. In such circumstances and taking into account the small differences between the structures in space groups $P6_3/mmc$ and $P6_3mc$, we first decided to perform refinements in the centrosymmetric space group at all pressures. The structural model in $P6_3/mmc$ ($Z = 2$) included isotropic thermal displacement parameters fixed to the values of reference 5 and not refined. The Na, V(1), V(2), V(3), O(1), O(2), and O(3) atoms are located at the Wyckoff sites 2c (1/3, 2/3, 1/4), 6g (1/2, 0, 0), 4e (0, 0, z), 2d (1/3, 2/3, 3/4), 12k (x, $2x$, z), 6h (x, $2x$, 3/4), and 4f (1/3, 2/3, z), respectively. The details of our structural refinement are presented in tables 1 and 2[5].

Our subsequent refinements in space group $P6_3mc$ allowing all possible positional parameters to vary freely did not lead to reasonable results due to the low *reflection-to-parameter* ratio. On the other hand, significance tests on the overall agreement factors based on the procedures suggested by Hamilton [19] for the centrosymmetric and the non-centrosymmetric models clearly demonstrated the latter to be superior at higher pressures.

To obtain more information about the $P6_3/mmc \rightarrow P6_3mc$ phase transition, we followed another strategy based on the assumption that the pressure- and temperature-induced structural changes are similar. Consequently, we analyzed the low-temperature *centrosymmetric* → *non-centrosymmetric* phase transition [4, 5] using the symmetry-mode analysis as described in [20–22][6]. This allowed us to single out the most

Table 1. Experimental data for the single-crystal measurements at different pressures using the model of the average structure $P6_3/mmc$ ($Z = 2$).

	0.49 GPa	2.60 GPa	4.20 GPa
Crystal data			
a (Å)	5.708(2)	5.687(2)	5.673(2)
c (Å)	13.074(6)	13.021(6)	12.974(6)
V (Å^3)	368.9(4)	364.7(4)	361.6(4)
ρ (g cm^{-3})	4.5415	4.5937	4.6332
μ (mm^{-1})	7.413	7.498	7.563
Data collection			
No. measured refl.	365	387	366
Range of hkl	$-4 \leqslant h \leqslant 5$	$-5 \leqslant h \leqslant 5$	$-4 \leqslant h \leqslant 5$
	$-5 \leqslant k \leqslant 5$	$-4 \leqslant k \leqslant 4$	$-5 \leqslant k \leqslant 5$
	$-12 \leqslant l \leqslant 13$	$-12 \leqslant l \leqslant 12$	$-12 \leqslant l \leqslant 12$
No. unique refl.	97	97	90
No. observed refl.[a]	58	63	51
$R(\text{int})^{\text{b}}_{\text{obs/all}}$	5.48/7.56	7.19/8.64	6.43/8.83
$\sin(\theta)/\lambda$	0.5015	0.5036	0.5053
Refinement[b]			
R_{obs}	8.58	8.61	7.87
wR_{obs}	7.50	7.54	7.75
R_{all}	14.93	13.86	14.95
wR_{all}	7.74	7.81	8.10
$\text{Go}F_{\text{all}}$	2.66	2.69	2.46
$\text{Go}F_{\text{obs}}$	3.45	3.31	3.25
No. parameters	6	6	6

[a] Criterion for observed reflections is $|F_{\text{obs}}| > 3\sigma$.
[b] All agreement factors are given in %, weighting scheme $1/[\sigma^2(F_{\text{obs}}) + (0.01F_{\text{obs}})^2]$.

Table 2. Positional parameters from single-crystal refinements for the average structure $P6_3/mmc$ ($Z = 2$). The estimated standard deviations are in brackets.

Coordinate	0.49 GPa	2.60 GPa	4.20 GPa
z [V(2)]	0.1470(7)	0.1483(6)	0.1488(7)
x [O(1)]	0.169(4)	0.170(4)	0.173(4)
z [O(1)]	0.077(1)	0.080(1)	0.080(2)
x [O(2)]	0.146(4)	0.155(4)	0.158(5)
z [O(3)]	0.590(3)	0.590(3)	0.594(3)

[5] Further details of the crystallographic investigations can be obtained from the Fachinformationszentrum Karlsruhe, D-76344 Eggenstein-Leopoldshafen, Germany, on quoting the depository numbers CSD 419547-419552.

[6] The symmetry-mode analysis could be carried out using the program AMPLIMODES on the Bilbao Crystallographic Server, http://www.cryst.ehu.es (see appendix).

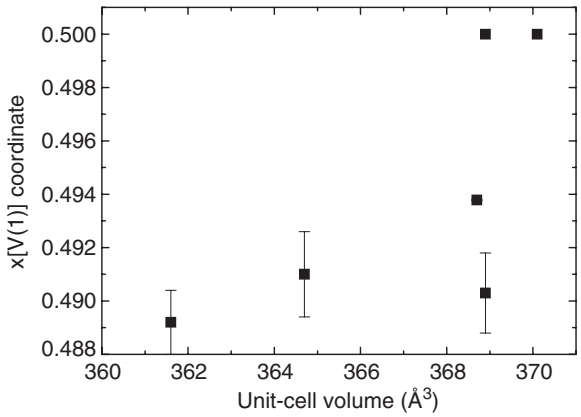

Figure 4. x [V(1)] coordinates as a function of the unit-cell volumes. The data point at 370.1 Å^3 corresponds to the high-symmetry phase ($P6_3/mmc$). The two data points at 368.9 Å^3 correspond to $P6_3/mmc$ and $P6_3mc$ symmetries. The data point at 368.7 Å^3 ($P6_3mc$) is taken from [4].

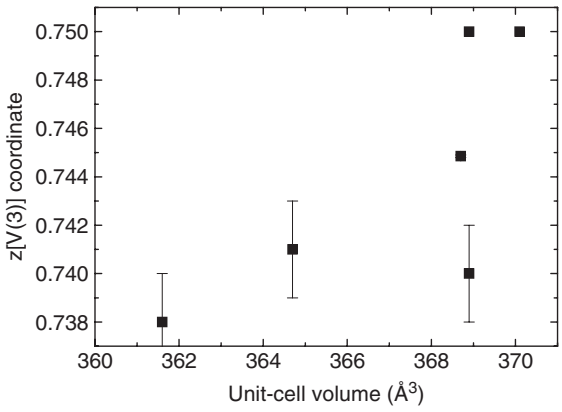

Figure 5. z [V(3)] coordinates as a function of the unit-cell volumes. The data point at 370.1 Å^3 corresponds to the high-symmetry phase ($P6_3/mmc$). The two data points at 368.9 Å^3 correspond to $P6_3/mmc$ and $P6_3mc$ symmetries. The data point at 368.7 Å^3 ($P6_3mc$) is taken from [4].

Table 3. Details of different refinements of the single-crystal data at different pressures. All agreement factors are given in %.

	R_{obs}	wR_{obs}	R_{all}	wR_{all}	No. parameters
			0.49 GPa		
$P6_3/mmc$	8.58	7.50	14.93	7.74	6
$P6_3mc$	7.87	6.55	17.84	7.01	9
$P\bar{6}2c$	9.46	7.79	17.72	8.08	9
			2.60 GPa		
$P6_3/mmc$	8.61	7.54	13.85	7.81	6
$P6_3mc$	8.36	7.15	15.56	7.46	9
$P\bar{6}2c$	8.46	7.03	15.08	7.34	9
			4.20 GPa		
$P6_3/mmc$	7.87	7.75	14.95	8.10	6
$P6_3mc$	6.76	6.12	15.57	6.53	9
$P\bar{6}2c$	7.15	6.30	18.07	6.89	9

important contributions of individual primary modes to the overall structural distortion. The most important contributions are related to the shift of the V(1) atom out of its special position (1/2, 0, 0) in $P6_3/mmc$ to the position $(x, 2x, 0)$ in space group $P6_3mc$ and the movement of V(3) out of the special position (1/3, 2/3, 3/4) to the position (1/3, 2/3, z) in space group $P6_3mc$. The third mode in importance corresponds to the movement of the Na atom from its special position (1/3, 2/3, 1/4) in the high-temperature phase to the position (1/3, 2/3, z) in the low-temperature phase.

We performed constrained refinements of the high-pressure data in space group $P6_3mc$, using only the three additional parameters x[V(1)], z[V(3)], and z[Na], while all others were fixed at the ideal values derived from the coordinates of the average structure $P6_3/mmc$ for the respective pressures (table 2). The results showed that only the introduction of the two x[V(1)] and z[V(3)] parameters leads to a substantial lowering of the overall agreement factors, while the refinement of the z coordinate of the Na atom shows no significant deviation from the ideal value of

Table 4. Refined coordinates of the V(1) and V(3) atoms in the low-symmetry phase of NaV_6O_{11} ($P6_3mc$, $Z = 2$).

Coordinate	0.49 GPa	2.60 GPa	4.20 GPa
x [V(1)]	0.490(2)	0.491(2)	0.489 (1)
z [V(3)]	0.740(2)	0.741(2)	0.738(2)

0.25 (tables 3 and 4)[7]. As a test, we also included other parameters in the refinement (i.e., secondary modes) but could not obtain better agreement factors. We are thus confident that the distortion corresponding to the symmetry reduction $P6_3/mmc \rightarrow P6_3mc$ is already very well described just by using the shifts of the V(1) and V(3) atoms. As seen in figures 4 and 5, the x coordinate of the atom V(1) and the z coordinate of the atom V(3) clearly diverge from the ideal values with decreasing unit-cell volumes, if one supposes that the data point corresponding to a pressure of 0.49 GPa ($V = 368.9$ Å^3) is erroneous. This might very well be the case, as this pressure might be below the critical pressure and it is quite likely that NaV_6O_{11} is still centrosymmetric.

Interatomic distances and polyhedral volumes [18] for the average structure in space group $P6_3/mmc$ at the different pressures are listed in tables 5 and 6. Except for the distances V(1)–O and V(3)–O, all the distances and parameters in table 5 as well as the polyhedral volumes in table 6 are identical in space groups $P6_3/mmc$ and $P6_3mc$ (table 7). The V(1)–O and V(3)–O(3) average distances in space group $P6_3mc$ are equal to the corresponding distances in space group $P6_3/mmc$.

The volume of the $V(1)O_6$ octahedron (table 6) is almost independent of the pressure, which suggests that the valence of the V(1) cation does not change significantly on compression. On the other hand, the $V(2)O_6$ octahedron expands,

[7] Table 3 shows the overall agreement factors for refinements in space groups $P6_3/mmc$, $P6_3mc$, and $P\bar{6}2c$, where the model in $P6_3mc$ was constrained. It can be seen that the results in $P6_3mc$ are clearly superior to the models in the other space groups.

Table 5. Structural parameters (Å) of various structural units at different pressures for the average structure $P6_3/mmc$ ($Z = 2$). The estimated standard deviations are in brackets.

Distance		0.49 GPa	2.60 GPa	4.20 GPa
NaO_{12} dodecahedra				
Na–O(1)	(x6)	2.79(3)	2.74(2)	2.71(3)
Na–O(2)	(x6)	2.86(3)	2.85(3)	2.84(3)
Average Na–O		2.82	2.80	2.78
$V(1)O_6$ Kagomé lattice				
V(1)–O(1)	(x4)	1.92(5)	1.93(4)	1.91(5)
V(1)–O(3)	(x2)	2.03(2)	2.02(2)	2.04(2)
Average V(1)–O		1.96	1.96	1.95
O(1)–O(1)	(x2)	2.81(4)	2.79(4)	2.72(4)
	(x2)	2.61(5)	2.67(4)	2.68(5)
O(1)–O(3)	(x4)	2.72(4)	2.74(4)	2.74(4)
	(x4)	2.86(3)	2.85(3)	2.84(3)
Average O–O		2.76	2.77	2.76
$V(2)O_6$ dimers				
V(2)–O(1)	(x3)	1.91(4)	1.89(3)	1.93(4)
V(2)–O(2)	(x3)	1.98(4)	2.02(3)	2.04(3)
Average V(2)–O		1.94	1.96	1.98
O(1)–O(1)	(x3)	2.89(4)	2.89(4)	2.95(4)
O(1)–O(2)	(x6)	2.76(4)	2.79(4)	2.75(4)
O(2)–O(2)	(x3)	2.51(6)	2.64(6)	2.69(4)
Average O–O		2.73	2.78	2.78
V(2)–V(2)		2.69	2.65	2.63
$V(3)O_5$ trigonal bipyramids				
V(3)–O(2)	(x3)	1.85(4)	1.76(4)	1.72(4)
V(3)–O(3)	(x2)	2.09(3)	2.08(3)	2.03(4)

Table 6. Comparison of polyhedral volumes (Å^3) at different pressures for the average structure $P6_3/mmc$ ($Z = 2$).

Polyhedron	0.49 GPa	2.60 GPa	4.20 GPa
NaO_{12}	52(1)	50(1)	50(1)
$V(1)O_6$	9.9(3)	10.0(3)	10.0(3)
$V(2)O_6$	9.5(3)	9.8(3)	10.1(3)
$V(3)O_5$	6.2(3)	5.6(3)	5.2(3)

but the $V(3)O_5$ polyhedron shrinks at the same time. In addition, the V(2)–V(2) distance diminishes (table 5). These observations suggest a possibility of a pressure-induced electron transfer from the V(3) to the V(2) cations. Together with the diminishing length of the face-sharing $V(2)O_6$ octahedral dimers and the increasing distortions of the NaO_{12} dodecahedra, the volume changes of the $V(3)O_5$ trigonal bipyramids are responsible for the anisotropic compressibility of NaV_6O_{11}.

The low-temperature structural investigations at ambient pressure have shown that the regular Kagomé lattice of the V(1) atoms is broken during the phase transitions $P6_3/mmc \rightarrow P6_3mc$ [4], as the V(1) atoms shift from their special positions to form V(1) trimers and the V(1)–V(1) distances split into inter-trimer and intra-trimer distances. Our constrained refinements of the high-pressure data in space group $P6_3mc$ and the low temperature study at 200 K [4] allow us to examine the unit-cell volume dependence of these distances (figure 6). As can be seen, the inter-trimer and

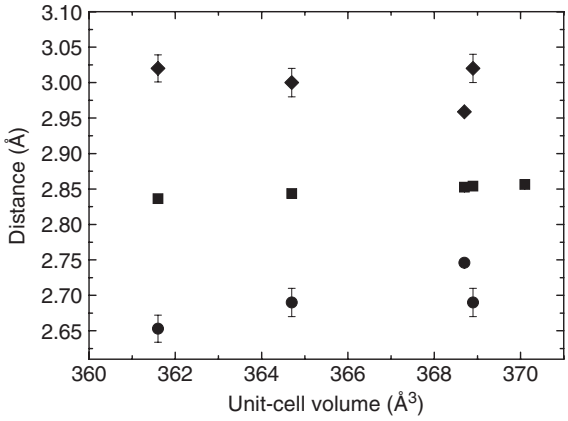

Figure 6. V(1)–V(1) distances as a function of the unit-cell volumes. Square symbols represent the distances in space group $P6_3/mmc$. Round and diamond symbols represent the intra-trimer and inter-trimer distances, respectively, in space group $P6_3mc$. The data points at 368.7 Å^3 ($P6_3mc$) are taken from [4].

Table 7. Interatomic distances (Å) at different pressures for the structure $P6_3mc$ ($Z = 2$). The estimated standard deviations are in brackets.

Distance		0.49 GPa	2.60 GPa	4.20 GPa
$V(1)O_6$ octahedra				
V(1)–O(1)	(x2)	1.88(1)	1.89(1)	1.86(1)
	(x2)	1.96 (2)	1.97(1)	1.96(1)
V(1)–O(3)		2.11(1)	2.09(1)	2.12(1)
		1.95(1)	1.95(1)	1.95(1)
Average V(1)–O		1.96	1.96	1.95
$V(3)O_5$ trigonal bipyramids				
V(3)–O(2)	(x3)	1.852(2)	1.764(2)	1.726(2)
V(3)–O(3)		1.95(3)	1.97(3)	1.88(3)
		2.22(3)	2.19(3)	2.18(3)
Average V(3)–O(3)		2.09	2.08	2.03

intra-trimer distances in the low-symmetry phase diverge from the V(1)–V(1) distances in the average structure $P6_3/mmc$ with decreasing unit-cell volumes. Again the data points obtained from the refinement of the single-crystal data at 0.49 GPa (368.9 Å^3) in the acentric space group suggest that the transition $P6_3/mmc \rightarrow P6_3mc$ has not yet taken place.

4. Conclusions

Our results show that the hexagonal lattice of NaV_6O_{11} is stable at least to 8.06 GPa at room temperature. The refinement of the high-pressure single-crystal data reveals the existence of a second-order $P6_3/mmc \rightarrow P6_3mc$ structural phase transition above 0.49 GPa, in good agreement with the earlier study [12], which suggested that the critical pressure at room temperature is above 1.15 GPa. No evidence for the occurrence of lower symmetry polymorphs has been observed. Hence, more work on the P-T structural and magnetic phase diagrams of NaV_6O_{11} is warranted.

The results of this study suggest that symmetry-mode analysis may serve as an aid for the structural refinement of both single-crystal and powder high-pressure diffraction data with limited information, i.e, with a small number of reflections. In the case of NaV_6O_{11}, the refinement could thus be limited to very few parameters to overcome the low *reflection-to-parameter* ratio. Given that the high-pressure data generally suffer from this kind of problems, the potential of symmetry-mode analysis for the structure determination and refinement should further be explored. This new approach could be applicable not only to displacive phase transitions but also to pseudosymmetric structures with a small distortion with respect to a configuration of higher symmetry [23, 24]. It should thus be possible to single out the contributions related to the primary modes, which reflect the symmetry reduction from the higher symmetrical phase. The parameters related to the secondary modes, which are supposed to be considerably less important [20–22], could then be excluded from the refinement to achieve a better *reflection-to-parameter* ratio.

Acknowledgments

We thank G Buth for his assistance at the Single Crystal Diffraction Beamline in the ANKA Angstroemquelle Karlsruhe. This work was supported by the European Community Research Infrastructure Action under the FP6-Programs: 'Structuring the European Research Area' through the Integrated Infrastructure Initiative 'Integrating Activity on Synchrotron and Free Electron Laser Science'; Contract RII3-CT-2004-506008 (IASFS). AG and KF acknowledge the Gobierno Vasco, the Ministerio de Ciencia y Tecnología, and the European Science Foundation for supporting their high-pressure laboratory.

Appendix

Symmetry-mode analysis for the $P6_3/mmc$ and $P6_3mc$ structures of NaV_6O_{11} at ambient pressure [4, 5] carried out using the program AMPLIMODES on the Bilbao Crystallographic Server, http://www.cryst.ehu.es.

High-symmetry structure

```
194
5.7123 5.7123 13.0974 90 90 120
7
V     1   6g    0.5 0.0 0.0
V     2   4e    0.0 0.0 0.14754
V     3   2d    0.3333333 0.6666667 0.75
O     1   12k   0.170520 0.341040 0.08043
O     2   6h    0.152730 0.305460 0.75
O     3   4f    0.3333333 0.6666667 0.59075
Na    1   2c    0.3333333 0.6666667 0.25
```

Low-symmetry structure

```
186
5.7123 5.7123 13.0974 90 90 120
10
V     1   6c    0.493780 0.987560 0
V     21  2a    0 0 0.14871
V     22  2a    0 0 0.35341
V     3   2b    0.3333333 0.6666667 0.74485
O     11  6c    0.171020 0.342040 0.08319
O     12  6c    0.169690 0.339380 0.42085
O     2   6c    0.152820 0.305640 0.74970
O     31  2b    0.3333333 0.6666667 0.58907
O     32  2b    0.3333333 0.6666667 0.90666
Na    1   2b    0.3333333 0.6666667 0.25490
```

Transformation matrix

```
[      1      0      0 ] [      0]
[      0      1      0 ] [      0]
[      0      0      1 ] [      0]
```

Transformed high-symmetry structure in the subgroup basis

```
186
5.712300 5.712300 13.097400 90.000000 90.000000 120.000000
10
V     1     6c    0.500000    0.000000    0.000000
V     2     2a    0.000000    0.000000    0.147540
V     2_2   2a    0.000000    0.000000    0.852460
V     3     2b    0.333333    0.666667    0.750000
O     1     6c    0.170520    0.341040    0.080430
O     1_2   6c    0.341040    0.170520    0.919570
O     2     6c    0.152730    0.305460    0.750000
O     3     2b    0.333333    0.666667    0.590750
O     3_2   2b    0.666667    0.333333    0.409250
Na    1     2b    0.333333    0.666667    0.250000
```

Atom pairings and distances

Atom mappings

WP	Atom	Coordinates in S_1	Atom	Coordinates in S_2
6c $(x, -x, z)$	V1	(1/2, 0, 0)	V1	(0.493 78, 0.987 56, 0)
2a $(0, 0, z)$	V2	(0, 0, 0.147 54)	V21	(0, 0, 0.148 71)
2a $(0, 0, z)$	V2_2	(0, 0, 0.852 46)	V22	(0, 0, 0.853 41)
2b $(1/3, 2/3, z)$	V3	(1/3, 2/3, 3/4)	V3	(1/3, 2/3, 0.744 85)
6c $(x, -x, z)$	O1	(0.170 52, 0.341 04, 0.080 43)	O11	(0.171 02, 0.342 04, 0.083 19)
6c $(x, -x, z)$	O1_2	(0.341 04, 0.170 52, 0.919 57)	O12	(0.339 38, 0.169 69, 0.920 85)
6c $(x, -x, z)$	O2	(0.152 73, 0.305 46, 3/4)	O2	(0.152 82, 0.305 64, 0.749 70)
2b $(1/3, 2/3, z)$	O3	(1/3, 2/3, 0.590 75)	O31	(1/3, 2/3, 0.589 07)
2b $(1/3, 2/3, z)$	O3_2	(2/3, 1/3, 0.409 25)	O32	(2/3, 1/3, 0.406 66)
2b $(1/3, 2/3, z)$	Na1	(1/3, 2/3, 1/4)	Na1	(1/3, 2/3, 0.254 90)

Atomic distances

WP	Atom	d_x	d_y	d_z	$\|d\|$
6c $(x, -x, z)$	V1	−0.0062	−0.0124	0.0000	0.0615
2a $(0, 0, z)$	V2	0.0000	0.0000	0.0012	0.0153
2a $(0, 0, z)$	V2_2	0.0000	0.0000	0.0009	0.0124
2b $(1/3, 2/3, z)$	V3	0.0000	0.0000	−0.0052	0.0675
6c $(x, -x, z)$	O1	0.0005	0.0010	0.0028	0.0365
6c $(x, -x, z)$	O1_2	−0.0017	−0.0008	0.0013	0.0187
6c $(x, -x, z)$	O2	0.0001	0.0002	−0.0003	0.0040
2b $(1/3, 2/3, z)$	O3	0.0000	0.0000	−0.0017	0.0220
2b $(1/3, 2/3, z)$	O3_2	0.0000	0.0000	−0.0026	0.0339
2b $(1/3, 2/3, z)$	Na1	0.0000	0.0000	0.0049	0.0642

Note: d_x, d_y and d_z are given in relative units. $|d|$ is the absolute distance given in Å.

Maximum atomic displacement in the distortion, Δ: 0.0675 Å.

After origin shift

Relative origin shift to eliminate a global displacement: (0.000 00, 0.000 00, 0.000 49).

Atom mappings

WP	Atom	Coordinates in S_1	Atom	Coordinates in S_2
6c $(x, -x, z)$	V1	(1/2, 0, 0)	V1	(0.493 78, 0.987 56, 0.999 51)
2a $(0, 0, z)$	V2	(0, 0, 0.147 54)	V21	(0, 0, 0.148 22)
2a $(0, 0, z)$	V2_2	(0, 0, 0.852 46)	V22	(0, 0, 0.852 92)
2b $(1/3, 2/3, z)$	V3	(1/3, 2/3, 3/4)	V3	(1/3, 2/3, 0.744 36)
6c $(x, -x, z)$	O1	(0.170 52, 0.341 04, 0.080 43)	O11	(0.171 02, 0.342 04, 0.082 70)
6c $(x, -x, z)$	O1_2	(0.341 04, 0.170 52, 0.919 57)	O12	(0.339 38, 0.169 69, 0.920 36)
6c $(x, -x, z)$	O2	(0.152 73, 0.305 46, 3/4)	O2	(0.152 82, 0.305 64, 0.74921)
2b $(1/3, 2/3, z)$	O3	(1/3, 2/3, 0.590 75)	O31	(1/3, 2/3, 0.588 58)
2b $(1/3, 2/3, z)$	O3_2	(2/3, 1/3, 0.409 25)	O32	(2/3, 1/3, 0.406 17)
2b $(1/3, 2/3, z)$	Na1	(1/3, 2/3, 1/4)	Na1	(1/3, 2/3, 0.254 41)

Atomic distances

WP	Atom	d_x	d_y	d_z	$\|d\|$
6c $(x, -x, z)$	V1	−0.0062	−0.0124	−0.0005	0.0619
2a $(0, 0, z)$	V2	0.0000	0.0000	0.0007	0.0089
2a $(0, 0, z)$	V2_2	0.0000	0.0000	0.0005	0.0060
2b $(1/3, 2/3, z)$	V3	0.0000	0.0000	−0.0056	0.0739
6c $(x, -x, z)$	O1	0.0005	0.0010	0.0023	0.0301
6c $(x, -x, z)$	O1_2	−0.0017	−0.0008	0.0008	0.0132
6c $(x, -x, z)$	O2	0.0001	0.0002	−0.0008	0.0104
2b $(1/3, 2/3, z)$	O3	0.0000	0.0000	−0.0022	0.0284
2b $(1/3, 2/3, z)$	O3_2	0.0000	0.0000	−0.0031	0.0403
2b $(1/3, 2/3, z)$	Na1	0.0000	0.0000	0.0044	0.0578

Note: d_x, d_y and d_z are given in relative units. $|d|$ is the absolute distance given in Å.

Maximum atomic displacement in the distortion, Δ: 0.0739 Å.

Symmetry modes summary

Atoms	WP	Modes	Show Modes
O1	12k	GM1 + (2)GM2 − (2)	Show
O2	6h	GM1 + (1)GM2 − (1)	Show
V1	6g	GM2 − (2)	Show
O3	4f	GM1 + (1)GM2 − (1)	Show
V2	4e	GM1 + (1)GM2 − (1)	Show
V3	2d	GM2 − (1)	Show
Na1	2c	GM2 − (1)	Show

Irrep: GM1+

Isotropy Subgroup: 194 P6_3/mmc D6h-4

The amplitude of this distortion is $Q_{\mathrm{GM1+}} = 0.0363$ Å.

Normalized polarization vector (in terms of the amplitudes of the (normalized) atomic symmetry modes).

V2 1	O1 1	O1 2	O2 1	O3 1
0.0795	0.9261	−0.1560	−0.0601	0.3288

Note: a second number next to the label counts the different symmetry modes that may happen for that orbit.

Normalized polarization vector expressed as displacements (in cell relative units) of the atoms in the asymmetric unit of the structure (normalization unit: 1 Å).

Atom	δx	δy	δz
V1	0.0000	0.0000	0.0000
V2	0.0000	0.0000	0.0030
V2_2	0.0000	0.0000	−0.0030
V3	0.0000	0.0000	0.0000
O1	−0.0046	−0.0091	0.0204
O1_2	−0.0091	−0.0046	−0.0204
O2	0.0025	0.0050	−0.0000
O3	0.0000	0.0000	0.0126
O3_2	0.0000	0.0000	−0.0126
Na1	0.0000	0.0000	0.0000

Virtual structure with only this symmetry component of the distortion frozen.

Irrep: GM2-

Isotropy Subgroup: 186 P6_3mc C6v-4

The amplitude of this distortion is $Q_{\mathrm{GM2-}} = 0.2269$ Å.

Normalized polarization vector (in terms of the amplitudes of the (normalized) atomic symmetry modes).

V1 1	V1 2	V2 1	V3 1	O1 1	O1 2	O2 1	O3 1	Na1 1
−0.0693	−0.6643	0.0658	−0.4604	0.3059	0.1004	−0.1117	−0.3030	0.3600

Note: a second number next to the label counts the different symmetry modes that may happen for that orbit.

Normalized polarization vector expressed as displacements (in cell relative units) of the atoms in the asymmetric unit of the structure (normalization unit: 1 Å).

Atom	δx	δy	δz
V1	−0.0274	−0.0548	−0.0022
V2	0.0000	0.0000	0.0025
V2_2	0.0000	0.0000	0.0025
V3	0.0000	0.0000	−0.0249
O1	0.0029	0.0059	0.0067
O1_2	−0.0059	−0.0029	0.0067
O2	0.0000	0.0000	−0.0035
O3	0.0000	0.0000	−0.0116
O3_2	0.0000	0.0000	−0.0116
Na1	0.0000	0.0000	0.0194

Virtual structure with only this symmetry component of the distortion frozen.

References

[1] de Roy M E, Besse J P, Chevalier R and Gasperin M 1987 *J. Solid State Chem.* **67** 185
[2] Kanke Y, Takayama-Muromachi E, Kato K and Matsui Y 1990 *J. Solid State Chem.* **89** 130
[3] Uchida Y, Kanke Y, Takayama-Muromachi E and Kato K 1991 *J. Phys. Soc. Japan* **60** 2530
[4] Kanke Y, Izumi F, Morii Y, Akiba E, Funahashi S, Kato K, Isobe M, Takayama-Muromachi E and Uchida Y 1994 *J. Solid State Chem.* **112** 429
[5] Kanke Y, Kato K, Takayama-Muromachi E and Isobe M 1992 *Acta Crystallogr.* C **48** 1376
[6] Uchida Y, Onoda Y and Kanke Y 2001 *J. Magn. Magn. Mater.* **226** 446
[7] Kanke Y 1999 *Phys. Rev.* B **60** 3764
[8] Iwata M and Ishibashi Y 1998 *J. Phys. Soc. Japan* **67** 691
[9] Akiba A, Yamada H, Matsuo R, Kanke Y, Haeiwa T and Kita E 1998 *J. Phys. Soc. Japan* **67** 1303
[10] Seo D K and Whangbo M H 1996 *J. Am. Chem. Soc.* **118** 3951
[11] Villesuzanne A, Whangbo M-H and Koo H-J 2005 *Chem. Mater.* **17** 4344
[12] Naka T, Matsumoto T, Kanke Y and Murata K 1995 *Physica* B **206/207** 853
[13] Piermarini G J, Block S, Barnett J D and Forman R A 1975 *J. Appl. Phys.* **46** 2774
Mao H K, Xu J and Bell P M 1986 *J. Geophys. Res.* **91** 4673
[14] Angel R J 1993 *J. Phys.: Condens. Matter* **5** L141
[15] Ahsbahs H 1995 *Z. Kristallogr.* (Suppl. 9) 42
Ahsbahs H 2004 *Z. Kristallogr.* **219** 305
[16] Angel R J, Bujak M, Zhao J, Gatta G D and Jacobsen S D 2007 *J. Appl. Crystallogr.* **40** 26
[17] Petricek V, Dusek M and Palatinus L Jana2000 *The Crystallographic Computing System* (Praha: Institute of Physics)
[18] Balic-Zunic T and Vickovic I 1996 *J. Appl. Crystallogr.* **29** 305
[19] Hamilton W C 1965 *Acta Crystallogr.* **18** 502
[20] Pérez-Mato J M, Gaztelua F, Madariaga G and Tello M J 1986 *J. Phys. C: Solid State Phys.* **19** 1923
[21] Aroyo M and Pérez-Mato J M 1998 *Acta Crystallogr.* A **54** 19–30
[22] Friese K, Aroyo M, Schwalowsky L, Adiwidjaja G and Bismayer U 2002 *J. Solid State Chem.* **165** 136
[23] Grzechnik A, Crichton W A, Marshall W G and Friese K 2006 *J. Phys.: Condens. Matter* **18** 3017
[24] Grzechnik A, Gesland J-Y and Friese K 2007 *J. Phys.: Condens. Matter* **19** 096215